Longshore current dislocation on barred beaches

A. K. Barreiro

Department of Mathematics, University of Illinois at Urbana-Champaign, Urbana, IL, USA

O. Bühler

Courant Institute of Mathematical Sciences, New York University, New York, NY, USA

A.K. Barreiro, Department of Mathematics, University of Illinois at Urbana-Champaign, 1409 W. Green St., Urbana, IL 61801, USA. (abarreir@uiuc.edu)

O. Bühler, Courant Institute of Mathematical Sciences, New York University, 251 Mercer St., New York, NY 10012, USA. (obuhler@cims.nyu.edu)

Abstract. We present a numerical investigation of longshore currents driven by breaking waves on barred beaches. Alongshore inhomogeneity in the wave envelope or bathymetry leads to the generation of strong dipolar structures when the waves are breaking. The dynamics of these structures transfers momentum from the bar of the beach into the trough. This study is pursued using a new model that allows long simulation times and realistic wave amplitudes. We study two idealized settings that are expected to produce current dislocation, as observed in field experiments. In one setting the current maximum is dislocated; in the other, the current is diffused but the maximum is not shifted.

1. Introduction

It is well known that the breaking of obliquely incident sea waves on a beach can generate a current running in the alongshore direction. These currents can feed rip currents, cause beach erosion, and their incorrect prediction can derail water borne military actions. A quantitative theory of this phenomenon was given by *Longuet-Higgins* (1970a,b). The forcing due to surface waves incoming from the open sea is modelled using the radiation stress theory developed earlier by *Longuet-Higgins and Stewart* (1960, 1961, 1962, 1963, 1964), wherein surface gravity waves are found to impart a vertically-averaged momentum flux to the flow. Breaking and other dissipative processes cause convergence of this momentum flux, and therefore a forcing on the mean flow. This force balances bottom friction and a modelled turbulent mixing; assuming that the mean current, bathymetry and wave forcing do not vary in the alongshore direction, this theory yields a one-dimensional momentum balance which can be solved for the longshore current.

The general prediction of Longuet-Higgins is that alongshore current should develop in areas of wave breaking. The qualitative features of this current depend on the bathymetry of the beach, as well as the model for wave-breaking. On a planar beach, the current will have its maximum at the offshore onset of wave breaking, and will decrease in magnitude closer to the shoreline. On a barred beach, generally waves break as they slow down and increase in height over the bar, but then subside as the water depth increases into the trough, and break again as they approach the shoreline. Therefore there should be a current on top of the bar and another closer to the shoreline.

The one-dimensional momentum balance has been used with varying degrees of success to predict currents in field and laboratory settings. Field experiments have been performed at Santa Barbara in 1980, Duck NC in 1990, 1994, and 1997, and Edmonds, the Netherlands in 1995. The first beach is generally planar, the others generally barred (bathymetry naturally shifts over the course of the experiment). A one-dimensional model essentially like that of Longuet-Higgins is used with some success to match the data collected in Santa Barbara (*Thornton and Guza*, 1986). Predicted currents are broad and have a single maximum that is reasonably near (typically shorewards of) the experimental current maximum on a cross-shore transect.

On the barred beaches, however, the record is mixed. A laboratory experiment that explicitly enforced alongshore homogeneity (*Reniers and Battjes*, 1997) in the mean current and wavetrain on barred beaches found that two maxima developed, one over the bar and another near the shore, and that one-dimensional models that include surface rollers and an eddy viscosity could accurately reproduce the observed bar current. In field settings, however, the location of the alongshore current maximum varies significantly, from the crest of the bar to the trough. The most striking discrepancies occur in the DELILAH (*Berkemeier et al.*, 1997) experiment, where the alongshore current has a single maximum close to the trough of the beach for most days when there is a distinct alongshore bar in place (*Church and Thornton*, 1993).

One hypothesis for the discrepancy is that there are momentum terms that are missing or inaccurately modelled. Most researchers now alter the radiation stress through the inclusion of a surface roller (*Svendsen*, 1984), an aerated body of water, produced by the overturning wave, which travels on top of the shoreward-traveling wave. The shear stress between the roller and the underlying wave dissipates energy and erodes the roller. Therefore momentum is first transferred to the roller, and then to the mean flow as the roller subsides. The overall effect is to delay the transfer of momentum from the breaking wave to the current. While this improves fits on planar beaches (and on a laboratory barred beach), it is not sufficient to cause the large dislocation observed in the field. Another proposal is that additional momentum fluxes can arise through "shear waves" resulting from a shear instability of a steady alongshore uniform current (*Bowen and Holman*, 1989; *Allen et al.*, 1996; *Slinn et al.*, 1998). *Slinn et al.* (1998) hypothesized that such instabilities could cause the cross-shore transport of alongshore momentum into the trough. They examine instabilities that arise in a realistic physical regime on an idealized barred beach. While the current is diffused into the trough region, the current *maxima* are not shifted in this study, as required to replicate the DELILAH results.

A second source of discrepancy between theory and experiment is in the assumption of alongshore homogeneity. Longuet-Higgins assumes that the bathymetry, mean current, and wave-train are alongshore homogeneous. Alongshore variations in the bathymetry (such as inhomogeneity in bar formations as has been observed in barrier islands) or wave forcing would cause the radiation stress to be nonhomogeneous and necessitate a two-dimensional momentum balance or evolution. The fact that a successful barred beach laboratory experiment was performed when alongshore variation is controlled is evidence that the LH theory is adequate under these circumstances.

We propose to examine the effect of alongshore nonhomogeneous wave-breaking on the development of currents on a barred beach. This inhomogeneity could be in the wave field itself, or produced by shoaling over nonhomogeneous bathymetry. The non-uniform breaking forces vortex dipoles in the mean flow, whose evolution inherently promotes dislocation of current on barred beaches, but not on planar beaches.

This effect was proposed by *Bühler and Jacobson* (2001) and tested using a non-linear shallow water model with explicit resolution of surface gravity waves. The high computational cost of this model did not enable the authors to simulate over the time scales used in field experimentaton. In this paper, we use a rigid-lid model, coupled with paramatrized gravity wave dynamics, to confirm and extend these results in a more realistic setting.

2. Vortex Dynamics

Oblique waves breaking on a beach will impart not only longshore momentum but vorticity as well. Generically, if there is alongshore variation in the height of the wave, vortex dipole structures will be produced (*Peregrine*, 1998, 1999; *Bühler*, 2000). In the case of a single isolated wave packet, we can model the breaking wave as a turbulent bore. It has been demonstrated that the circulation produced around the edges of a bore of finite extent is proportional to the energy dissipation, but where the sign of the circulation depends on which edge is being considered (*Peregrine*, 1998).

How may the alongshore variations arise? One mechanism is through directional and frequency spreading of the incoming wave group. A second mechanism is thorough non-uniform bathymetry, which will produce variability because of differential shoaling and possibly focusing effects. Once reaching the bar, a variable wave train will break at some locations along the bar (where the envelope is high enough to become unstable) and fail to break, or break weakly, at others. Each isolated location of breaking will produce a dipole vorticity structure.

Now let us consider the dynamics of a vortex dipole on a sloping beach. We will idealize the dipolar structure as a pair of circular vortices with oppositely signed circulations. The vortex dynamics is a shallow, low-Froude number flow; the typical flow speed is small compared to the gravity wave speed. A reasonable approximation to this flow is to neglect surface deflections by using the shallow water equations with a rigid lid

$$\nabla \cdot (h_S \boldsymbol{u}) = 0 \tag{1}$$

$$\frac{D\boldsymbol{u}}{Dt} + \frac{1}{\rho}\nabla p = 0 \tag{2}$$

where h_S is the still water depth, p is the pressure at the rigid lid, and ρ is the fluid density (which we will always take to be constant). The bottom boundary conditions are free-slip.

The flow described by these equations satisifes Kelvin's circulation theorem; the circulation around a material loop (e.g. the boundary of an isolated vortex) will remain constant under the evolution of this flow. This implies the material conservation of potential vorticity (in the absence of forcing or dissipation); that is,

$$q \equiv \frac{\nabla \times \boldsymbol{u}}{h} \tag{3}$$

$$\frac{Dq}{Dt} = 0 \tag{4}$$

There are several dynamical effects present that may effect the evolution of the vortices. The shallow water approximation assumes that there is no vertical variation in vorticity or velocity; therefore the usual two-dimensional vortex dynamics are active (*Chorin and Marsden*, 1993). For example, two vortices of the same sign will tend to rotate about their center of circulation, and two vortices of opposing sign will tend to mutually advect away, in a straight line if they are of equal magnitude. Vortices will also travel parallel to wall boundaries, a consequence of satisfying the no-normal-flow condition.

We also have a self-advection effect because of the sloping bottom. On a planar beach, a well-known approximation to a small, circular region of constant vorticity is that of an axisymmetric vortex ring. A vortex that takes the form of a circular arc will have motion identical to the corresponding vortex ring. The motion of a vortex ring is along its center axis and may be characterized in terms of its circulation (Γ) and inner and outer radii (b and R respectively).

The velocity, according to *Lamb* (1932), is given by

$$U = \frac{\Gamma}{4\pi R}\left(\ln\left(\frac{8R}{b}\right) - \frac{1}{4}\right) \tag{5}$$

Translated to the planar beach, the equivalent vortex ring has outer radius $h/|\nabla h|$ and inner radius b; due to mass conservation we must have

$$b = b_0 \left(\frac{h_0}{h}\right)^{1/2} \tag{6}$$

where b_0 and h_0 are the original radius and water depth respectively, throughout the motion of the vortex. Using these identities the self-advection velocity U (5) may be written in terms of these physical variables as

$$U = \frac{\Gamma}{4\pi}\left(\frac{\nabla h}{h} \times \hat{z}\right)\left(\ln\left(\frac{8}{b_0 h_0^{1/2}}\frac{h^{3/2}}{|\nabla h|}\right) - \frac{1}{4}\right) \tag{7}$$

This makes clear that the direction of self-advection depends on both the circulation Γ and the direction of the gradient ∇h. One can verify from (7) that the vortex separation will increase as the vortex couple moves into deeper water, and decrease if the couple moves into shallower water, as shown in Figure 1. This approximation may also be used in the case of a non-planar beach, where the vortex ring is no longer an exact solution. We again use ∇h to determine the outer radius, but here it is a local slope. This expression (7) has been shown to be a leading order approximation for the law of motion for vortices of small dimensionless radius $O(\epsilon)$, separated by distances of $O(1)$ (*Richardson*, 2000).

Together, these two facts explain why a packet of breaking waves will create a dislocated current on a barred beach. First, a vortex dipole will be created at the location of the bar; or, on a planar beach, at the onset of breaking. The vortices by mutual advection will want to move shoreward. On a planar beach, self-advection will quickly move the vortices apart until their mutual advection is negligible.

On a barred beach, by contrast, the vortices will move closer together as they move shoreward. Therefore their shoreward motion is not arrested until the vortices climb out of the trough, separating now because the local slope of the topography has reversed (*Bühler and Jacobson*, 2001). The result is a dislocation of the corresponding alongshore momentum from the bar, the site of wave-breaking, to the trough, the eventual location of the vortices.

3. Numerical Model

We model the resolved vortical flow by the shallow water equations with a rigid lid in their velocity-stream formulation. $\boldsymbol{F}$ will refer to the radiation stress only; wind forcing is neglected, as in the surf zone it is generally thought to be much less important than wave forcing. $\boldsymbol{B}$ refers to the bottom friction term. The shallow-water equations with a rigid lid are

$$\nabla \cdot (h\boldsymbol{u}) = 0 \tag{8}$$

$$\frac{D\boldsymbol{u}}{Dt} + \frac{1}{\rho}\nabla p = \boldsymbol{F} - \boldsymbol{B} \tag{9}$$

in terms of the horizontal velocity $\boldsymbol{u} = (u, v)$, water depth $h(x, y)$, and pressure at the water surface p. Because of (8), there exists a scalar streamfunction ψ such that

$$\boldsymbol{u} = \frac{1}{h}\nabla^{\perp}\psi \tag{10}$$

If we define the scalar potential vorticity in terms of the vertical component of the vorticity,

$$q \equiv \frac{\nabla \times \boldsymbol{u}}{h}, \tag{11}$$

then ψ and q are related by the Poisson equation

$$\nabla \cdot \left(\frac{\nabla\psi}{h}\right) = hq \tag{12}$$

and the time evolution equation for q can be written as

$$\frac{\partial q}{\partial t} + \frac{1}{h}J(\psi, q) = \frac{\nabla \times \boldsymbol{F}}{h} - \frac{\nabla \times \boldsymbol{B}}{h}. \tag{13}$$

where the Jacobian $J(a, b) \equiv \frac{\partial a}{\partial x}\frac{\partial b}{\partial y} - \frac{\partial b}{\partial x}\frac{\partial a}{\partial y}$. We will numerically solve the equations (12) and (13) on the domain

$$0 \le x \le D \tag{14}$$

$$0 \le y \le L \tag{15}$$

with the following boundary conditions on (12):

$$\psi(x, y) = 0 \qquad x = 0 \tag{16}$$
$$\frac{\partial\psi}{\partial x}(x, y) = M\psi(x, y) \qquad x = D \tag{17}$$
$$\tag{18}$$

and $\psi(x, y) = \psi(x, y + L)$. M is a Dirichlet-to-Neumann map (*Keller and Givoli*, 1989; *Grote and Keller*, 1995). M is chosen to ensure that the solution to (12) on the bounded domain (14) is the restriction of a solution valid in the corresponding infinite domain $0 \leq x \leq \infty$, with the appropriate boundary conditions at infinity. The resulting velocity field does not "see" the presence of the boundary. The form of M will depend on assumptions made about the topography in the infinite domain; for the simulations in this paper, we assume that the topography is constant-depth for $x > D$.

Bottom friction can be well-approximated by a quadratic function of the free stream velocity $\overline{\boldsymbol{u}}$ (as in a turbulent boundary layer (*Kamphius*, 1975)); specifically

$$\boldsymbol{B} = \frac{c_f}{h} |\overline{\boldsymbol{u}}| \overline{\boldsymbol{u}}.$$

However, only the wave-averaged velocity field is represented in the numerical model. We seek an expression that includes both the quadratic mean-flow friction and an approximation to the littoral friction produced by the oscillating waves interacting with the mean current (as in *Longuet-Higgins* (1970a)).

We first decompose the instantaneous velocity field into the phase-averaged velocity and the wave velocity $\overline{\boldsymbol{u}} = \boldsymbol{u} + \boldsymbol{u}'$. We assume that $|\boldsymbol{u}| < |\boldsymbol{u}'|$, as in *Longuet-Higgins* (1970a). Assuming a simple wave structure we can derive an expression in terms of the wave vector and magnitude, which is linear in the wave-averaged velocity $\boldsymbol{u}$. If $|\boldsymbol{u}| > |\boldsymbol{u}'|$, then quadratic friction in $\boldsymbol{u}$ will predominate. Adding these together we have $\boldsymbol{B}$ as derived in *Bühler and Jacobson* (2001),

$$\boldsymbol{B} = \frac{c_f}{h_S} \frac{2}{\pi} u'_{max} \boldsymbol{u} \cdot \left(\boldsymbol{\delta} + \frac{\boldsymbol{k}\boldsymbol{k}}{\kappa^2} \right) + \frac{c_f}{h_S} |\boldsymbol{u}| \boldsymbol{u}$$

where $\boldsymbol{k}$ is the wave vector, $\kappa = |\boldsymbol{k}|$, and $u'_{\max}$ is the maximum orbital velocity of the waves. We use a constant friction coefficient c_f.

To summarize the numerical methods used, we first consider the dynamic equation (12). We use grid-based rather than pseudo-spectral methods due to the arbitrary nature of the topography. At each time step, the Jacobian $J(\psi, q)$ is computed using the Arakawa Jacobian. The friction term is computed using second-order differences. The time integration is performed using the leapfrog method, with an occasional Huen predictor-corrector step (as in *Merryfield et al.* (2001)) to control the computational mode. To solve the Poisson equation for ψ, two methods are employed depending on whether or not the bathymetry is y-independence. If it is, we can perform a fast direct inversion in Fourier space. If the bathymetry is two-dimensional, we use standard iterative multi-grid methods (*Hackbusch*, 1985).

The waves are modelled by a parameterization that resolves the rotational part of the momentum convergence of breaking waves. As observed in *Bühler and Jacobson* (2001) the radiation stress tensor appears in an asymptotic description of the shallow water equations with small-amplitude waves as a forcing on the averaged, vortical flow. The same expression was previously derived (*Longuet-Higgins and Stewart* (1964) and many others) as the excess momentum flux that occurs in the presence of waves. *Bühler and Jacobson* (2001) show that radiation stress can be decomposed as

$$-\frac{1}{h}\nabla \cdot \mathbf{S} \;=\; \frac{\partial \mathbf{p}}{\partial t} - F - \frac{1}{2}\nabla\overline{|\boldsymbol{u}'|^2} \tag{19}$$

If the waves are steady, we need only resolve

$$F \;=\; \frac{\boldsymbol{k}}{h}\nabla \cdot (\frac{\boldsymbol{k}}{\kappa^2}E). \tag{20}$$

where $\boldsymbol{k}$ and κ are as previously defined, and E is the wave energy per unit area. This expression only depends on the steady wave train. The necessary fields are computed using ray tracing. The derived wave equations (*Hayes*, 1970) are computed along each trajectory using the method of *White and Fornberg* (1998).

A saturation criterion is used to parametrize energy dissipation from breaking. As the wave energy per unit area (E) is computed along a wave trajectory, it is suppressed if the amplitude of the wave exceeds a fraction α of the still water depth h (i.e. if the wave saturates). The resulting energy profile is used in (20). We choose, as in *Longuet-Higgins* (1970a), $\alpha = 0.41$.

4. Numerical Simulations

We perform numerical simulations to demonstrate the feasibility of this mechanism. We compare the current forced by a isolated wave packet to that forced by a homogeneous wave train. We observe the response to both types of forcing on planar and barred beaches. The isolated packet should generate one vortex dipole (per periodic extension of the domain) and show current dislocation on a barred beach, but little or no dislocation on a planar beach. A homogeneous wave should show no dislocation on either beach.

The barred topography was chosen to smoothly vary so as to have a 1 meter-deep bar 100 meters from the shoreline, with a 2 meter-deep trough at 50 meters. After the bar, the water depth smoothly flattens to 4 meters. The “planar” topography is piecewise linear with a slope of about 1:30 until 125 meters away from shoreline, beyond which point the bottom is flat.

4.1. Homogeneous vs. inhomogeneous wave-train

The rotational component of a steady radiation stress is computed using ray-tracing from seaward boundary conditions on the wave amplitude. This amplitude is specified in terms of the alongshore coordinate and is either constant, or Gaussian with a width three times the wavelength. In both cases, the peak amplitude (comparable to the statistic H_{rms}) at the seaward boundary is 0.8 meters. The simulations are run for a total of 8 hours (simulation time); we observe both short and long time response of the current.

Simulations D and B then (homogeneous forcing and homogeneous topography) should show no current dislocation and should broadly satisfy the predictions of *Longuet-Higgins* (1970a,b). Simulation C (inhomogeneous wave forcing, but planar beach) should show modest dislocation, because the topography is not conducive to forward motion of vortices. Simulation A should show marked dislocation, with a preference for the local maximum of water depth.

The forcing profiles for the Gaussian packet shows the expected dipole pattern on both a barred beach (Figure (4)) and a planar beach (Figure (3)).

The early development of current is as expected. For homogeneous waves breaking on a barred beach (simulation B), the current develops over the bar, where its maximum is located for the entirety of the simulation; snapshots are shown in Figure 5. On a planar beach, the current initially develops at the location of wave breaking and shows a slight shift shoreward as the simulation progresses, consistent with the vortex dynamics (Figure 6). On a barred beach, the current initially develops on the bar, but shows a marked shift shorewards as the simulation progresses, with its maximum located at the bar trough (Figure 7).

There is a significant difference in the magnitude of the alongshore-averaged velocity between simulation B and simulations A and C. This can be attributed to the difference in alongshore-averaged momentum flux associated with the differing wave forcing. The alongshore-averaged momentum flux, as calculated offshore (say at 150 meters, before any wave breaking has occurred) is 9 times greater in the case of the homogeneous wavetrain; hence, the order of magnitude difference in velocity magnitudes.

The velocity profile in Figure 5 is relatively narrow and time-independent. We emphasize that this is an alongshore-averaged profile; a snapshot of the potential vorticity shows rippling associated with shear instability (Figure 8).

4.2. Long-time response

In the previous section, we examined the evolution of the nearshore current structure from rest over the period of about 2 hours. However, experimental field data is typically averaged from instantaneous measurements over a period of time comparable to this length of time (in DELILAH, current measurements were processed in 34 minute increments) and the current structure is relatively steady over a period of hours. So it is important to demonstrate that the mechanism for current dislocation that we have proposed can persist over a number of hours of simulation time, or even be a steady state.

We demonstrate this by plotting the alongshore-averaged alongshore velocity for a long-running version of simulation A. We see a persistent spike in velocity at the trough (50 meters), in Figure 9.

Over time, a secondary current develops outside of the surf zone (Figures 9 and 10). This current develops in simulations A and C (packet) but not B and D (homogeneous forcing) and is very pronounced in simulation A. This is a consequence of the peculiar vortex dynamics of the isolated packet; as the vortex dipole advects out of the trough and separates, it spins off small coherent vortices that travel down the beach until they meet their "mate" near the periodic boundary. These vortices now travel shorewards and transport some momentum offshore. Exacerbating this trend is a second circulation dipole generated at the shoreline; this circulation also gets swept offshore. This second dipole structure is an artifact of the isolated packet and we do not expect to see it in more general idealized or realistic models of wave dissipation forcing (for example, simulation E does not show this current).

4.3. Inhomogeneous bathymetry

We next consider alongshore variation from an idealized inhomogeneous bathymetry. We introduce an alongshore variation into the bar used for simulations A and B. The variation is such that the height of the bar relative to the trough varies from 0.2 meters to 1.0 meters over an alongshore distance of approximately 100 meters, which is consistent with the magnitude of bathymetry variations recorded during the DELILAH experiment. The wave forcing at the offshore boundary is uniform with an amplitude of 0.8 meters, as in simulations B and D.

The vorticity forcing profile (Figure 11) show dipoles over the bar where breaking is strengthened because of shoaling. Vorticity profiles during the simulation (Figure 13) show a vortex dipole signature extending into the bar trough; however there are also intense negative vortices spinning off in the seaward direction. This might be explained by comparing the forcing profile with that of simulation A: the negative vortex is forced primarily behind the peak of the bar, where the slope is such that the vortex will travel parallel and away from the site of strong breaking.

The alongshore-averaged current shows significant diffusion into the trough region (see Figure 12) compared with an alongshore homogeneous beach (Figure 7). However, the maximum of the current is still located at the bar peak.

5. Discussion

Our results in this study are mixed; an isolated wave packet produces current dislocation, but uniform waves on a varying bar topography produce current diffusion but not dislocation. A logical next step is to examine the response of this system to a random wave-train. *Dongeren et al.* (2003) use a wave driver which generates random wave trains that match the frequency-directional swell spectrum observed during the DELILAH experiment. The time-series in Figure 3 of *Dongeren et al.* (2003) shows a slowly varying envelope of surface elevation (above rest - i.e. amplitude); its magnitude varies in a oscillatory fashion to as little as 10% of its peak amplitude. We would guess that the vortex dipoles produced by such alongshore variation, either on a uniform beach or inhomogeneous beach, might produce dislocation. It is also a question whether or not a random wave field alone is enough to produce this behavior; a recent simulation of longshore currents under DELILAH field conditions found that current dislocation occured whether the wave field was uniform or random, suggesting that it was the bathymetry, or some other aspect of the simulation, that allowed bar trough currents (*Chen et al.*, 2003). We are interested in studying this question in our idealized setting.

A surprising feature of our simulations is that the vortex dynamics are essentially laminar; vortex mergers and an upscale energy cascade do not appear to occur. This is explained by recent turbulence studies with quadratic bottom friction that show that the frictional arrest number is linearly related to the quadratic drag coefficient but independent of the forcing strength. *Grianik et al.* (2004) find that the frictional arrest number in constant depth shallow water is well-approximated by

$$k_a \approx 51\frac{c_f}{h} \tag{21}$$

so long as the arrest scale and forcing scale are well-separated. In our simulation $c_f = 0.01$, so that the arrest scale relative to the water depth is about

$$k_a h \approx 0.5 \tag{22}$$

However, shallow-water dynamics assume that $kh < 1$; that is most dynamics in shallow-water, and therefore meter-scale or larger horizontal coastal dynamics, is at or below the arrest scale. One consequence is that vortices must be directly forced by inhomogeneous wave breaking, as they cannot arise from turbulent interactions such as vortex mergers.

6. Acknowledgements

This work was supported under NSF-OCE grant number 0324934.

References

Allen, J., P. Newberger, and R. Holman (1996), Nonlinear shear instabilities of alongshore currents on plane beaches, *Journal of Fluid Mechanics*, *310*, 181–213.

Berkemeier, W., et al. (1997), The 1990 DELILAH nearshore experiment: Summary report, *Tech. Rep. CHL-97-24*, U.S. Army Corps of Engineers, revised 2001.

Bowen, A., and R. Holman (1989), Shear instabilities of the mean longshore current. 1. Theory, *Journal of Geophysical Research*, *94*(C12), 18,023–18,030.

Bühler, O. (2000), On the vorticity transport due to dissipating or breaking waves in shallow-water flow, *Journal of Fluid Mechanics*, *407*, 235–262.

Bühler, O., and T. E. Jacobson (2001), Wave-driven currents and vortex dynamics on barred beaches, *Journal of Fluid Mechanics*, *499*, 313–339.

Chen, Q., J. Kirby, R. Dalrymple, F. Shi, and E. Thornton (2003), Boussinesq modeling of longshore currents, *Journal of Geophysical Research*, *108*(C11).

Chorin, A., and J. Marsden (1993), *A Mathematical Introduction to Fluid Mechanics*, 3rd ed., Springer.

Church, J., and E. Thornton (1993), Effects of breaking wave induced turbulence within a longshore current model, *Coastal Engineering*, *20*, 1–20.

Dongeren, A. V., A. Reniers, J. Battjes, and I. Svendsen (2003), Numerical modeling of infragravity wave response during delilah, *Journal of Geophysical Research*, *108*(C9).

Grianik, N., I. Held, K. Smith, and G. Vallis (2004), The effects of quadratic drag on the inverse cascade of two-dimensional turbulence, *Physics of Fluids*, *16*(1), 73–78.

Grote, M., and J. Keller (1995), On nonreflecting boundary conditions, *Journal of Computational Physics*, *122*, 231–243.

Hackbusch, W. (1985), *Multi-Grid Methods and Applications*, Springer Series in Computational Mathematics, Springer-Verlag.

Hayes, W. (1970), Kinematic wave theory, *Proceedings of the Royal Society of London, Series A*, *320*(1541), 209–226.

Kamphius, J. (1975), Friction factor under oscillatory waves, *Journal of the Waterways, Harbors and Coastal Engineering*, *101*, 135–144.

Keller, J., and D. Givoli (1989), Exact non-reflecting boundary conditions, *Journal of Computational Physics*, *82*, 172–192.

Lamb, H. (1932), *Hydrodynamics*, Dover Publications, Inc.

Longuet-Higgins, M. (1970a), Longshore currents generated by obliquely incident sea waves, 1, *Journal of Geophysical Research*, *75*(33), 6778–6789.

Longuet-Higgins, M. (1970b), Longshore currents generated by obliquely incident sea waves, 2, *Journal of Geophysical Research*, *75*(33), 6790–6801.

Longuet-Higgins, M., and R. Stewart (1960), Changes in the form of short gravity waves on long waves and tidal currents, *Journal of Fluid Mechanics*, *8*, 565–583.

Longuet-Higgins, M., and R. Stewart (1961), The changes in amplitude of short gravity waves on steady non-uniform currents, *Journal of Fluid Mechanics*, *10*, 529–549.

Longuet-Higgins, M., and R. Stewart (1962), Radiation stress and mass transport in gravity waves, with application to surf-beats, *Journal of Fluid Mechanics*, *13*, 481–504.

Longuet-Higgins, M., and R. Stewart (1963), A note on wave set-up, *Journal of Marine Research*, *21*, 4–10.

Longuet-Higgins, M., and R. Stewart (1964), Radiation stresses in water waves; a physical discussion, with applications, *Deep-Sea Research*, *11*, 529–562.

Merryfield, W., P. Cummins, and G. Holloway (2001), Equilibrium statistical mechanics of barotropic flow over finite topography, *Journal of Physical Oceanography*, *31*, 1880–1890.

Peregrine, D. (1998), Surf zone currents, *Theoretical and Computational Fluid Dynamics*, *10*, 295–309.

Peregrine, D. (1999), Large-scale vorticity generation by breakers in shallow and deep water, *European Journal of Mechanics; B, Fluids*, *18*, 403–408.

Reniers, A., and J. Battjes (1997), A laboratory study of longshore currents over barred and non-barred beaches, *Coastal Engineering*, *30*, 1–22.

Richardson, G. (2000), Vortex motion in shallow water with varying bottom topography and zero Froude number, *Journal of Fluid Mechanics*, *411*, 351–374.

Slinn, D., J. Allen, P. Newberger, and R. Holman (1998), Nonlinear shear instability of alongshore currents over barred beaches, *Journal of Geophysical Research*, *103*(C9).

Svendsen, I. (1984), Wave heights and set-up in a surf zone, *Coastal Engineering*, *8*, 303–329.

Thornton, E., and R. Guza (1986), Surf zone currents and random waves: Field data and models, *Journal of Physical Oceanography*, *16*, 1165–1178.

White, B., and B. Fornberg (1998), On the chance of freak waves at sea, *Journal of Fluid Mechanics*, *355*, 113–138.

7. Figure captions

Figure 1: Self-advection on a planar beach

Figure 2: $-\nabla \times F$ for simulation B. Because the forcing is alongshore homogenous, we present a single cross-shore transect.

Figure 3: $-\nabla \times F$ for simulation C

Figure 4: $-\nabla \times F$ for simulation A

Figure 5: Early development of alongshore-averaged longshore velocity for simulation B. The heavy line denotes the velocity profile at the time indicated in the subplot title. In subplots (b), (c), and (d), thinner lines indicate the earlier velocity profiles for comparison. A scaled plot of the bathymetry is shown below the zero velocity line.

Figure 6: Early development of alongshore-averaged longshore velocity for simulation C. The heavy line denotes the velocity profile at the time indicated in the subplot title. In subplots (b), (c), and (d), thinner lines indicate the earlier velocity profiles for comparison.

Figure 7: Early development of alongshore-averaged longshore velocity for simulation A. The heavy line denotes the velocity profile at the time indicated in the subplot title. In subplots (b), (c), and (d), thinner lines indicate the earlier velocity profiles for comparison.

Figure 8: Potential vorticity snapshot from simulation B.

Figure 9: Alongshore-averaged alongshore velocity for simulation A.

Figure 10: Alongshore-averaged alongshore velocity for simulation C.

Figure 11: $-\nabla \times F$ for simulation E

Figure 12: Early development of alongshore-averaged longshore velocity for simulation E. The heavy line denotes the velocity profile at the time indicated in the subplot title. In subplots (b), (c), and (d), thinner lines indicate the earlier velocity profiles for comparison.

Figure 13: Potential vorticity snapshots from simulation E

8. Tables

Parameter	Definition	Formula or value
CFL	Courant-Friedrichs-Levy number	< 0.9
Δt	Time step	$\frac{CFL}{\max\lvert\mathbf{u}\rvert}\frac{1}{1/\Delta x+1/\Delta y}s$
Δx	x (cross-shore)-grid spacing	$1\,m$
Δy	y (alongshore)-grid spacing	$1\,m$
D	Cross-shore dimension	$512\,m$
L	Alongshore dimension	$512\,m$
h_{S_0}	Still-water depth at seaward boundary	$4\,m$
a	Amplitude of waves at seaward boundary	$0.2\,h_{S_0}$
θ	Angle of incidence at seaward boundary	15
κ	Magnitude of wave-number vector at $x = 200m$	$0.29\,m^{-1}$
T	Wave period	3.45 s
c_f	Bottom friction coefficient	0.01

Table 1. Parameters common over simulations A,B,C,D,E

Simulation	Topography	Wave packet structure
A	Barred	Packet
B	Barred	Homogeneous
C	Linear	Packet
D	Linear	Homogeneous
E	Barred, y-dependent	Homogeneous

Table 2. Description of simulations

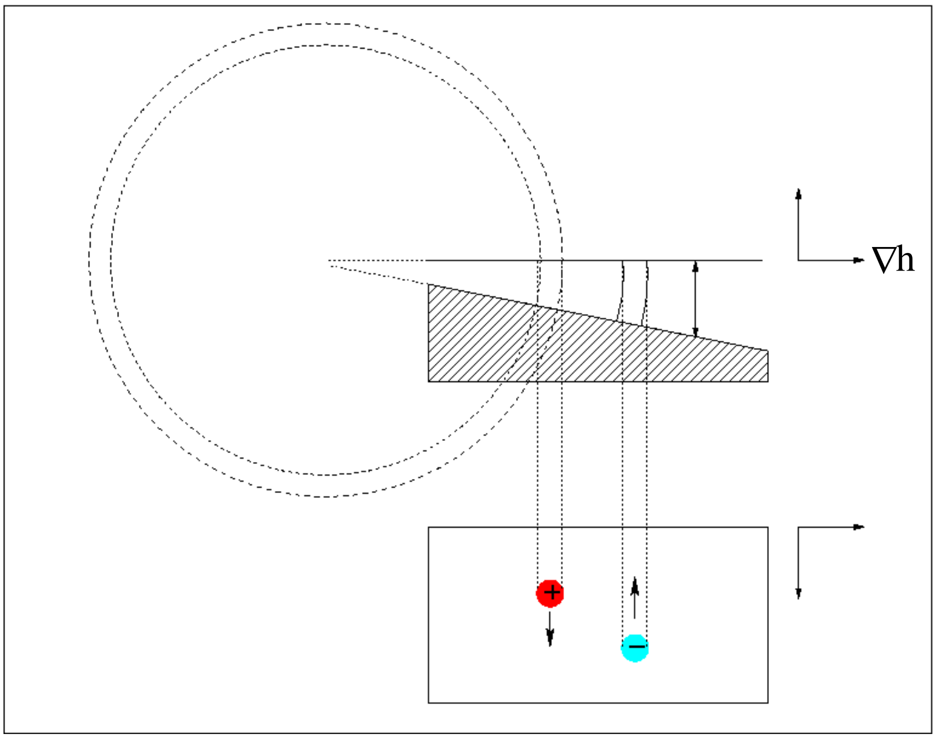

Figure 1. Self-advection on a planar beach

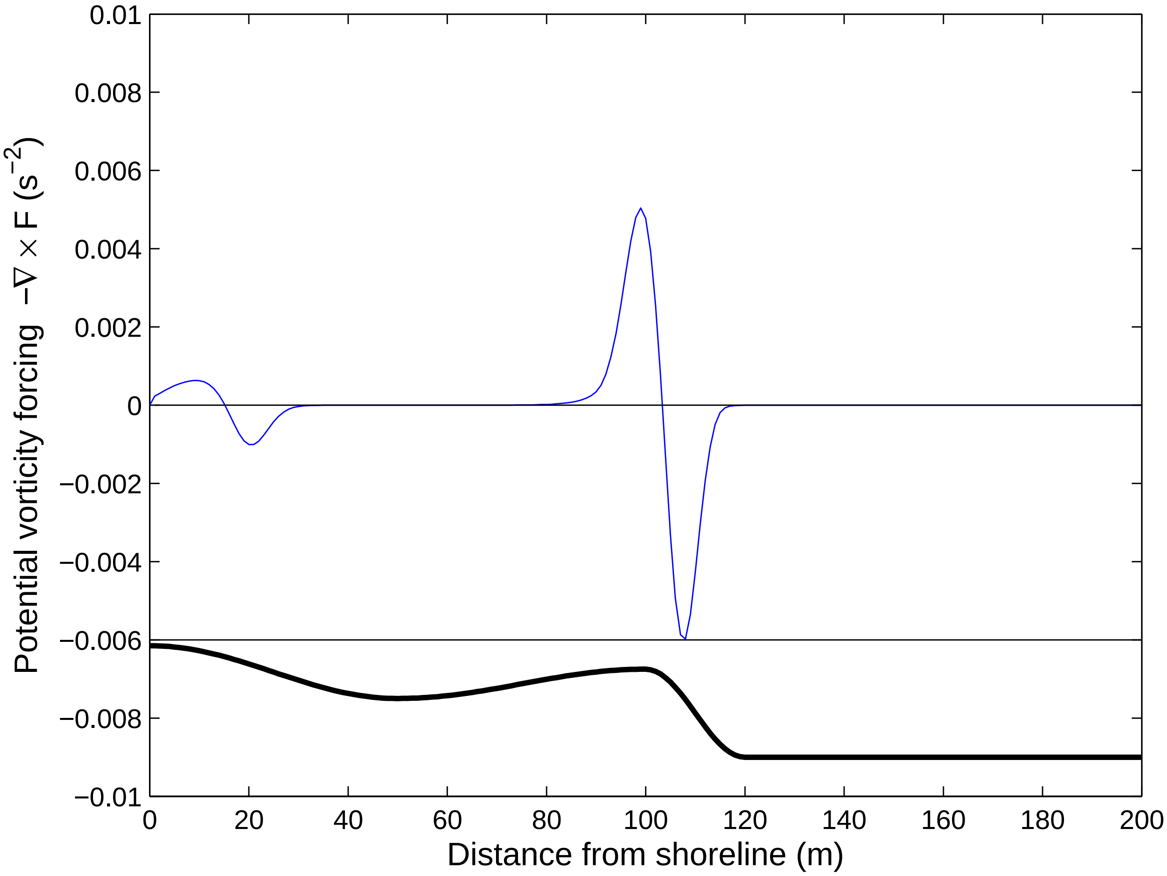

Figure 2. $-\nabla \times F$ for simulation B. Because the forcing is alongshore homogenous, we present a single cross-shore transect.

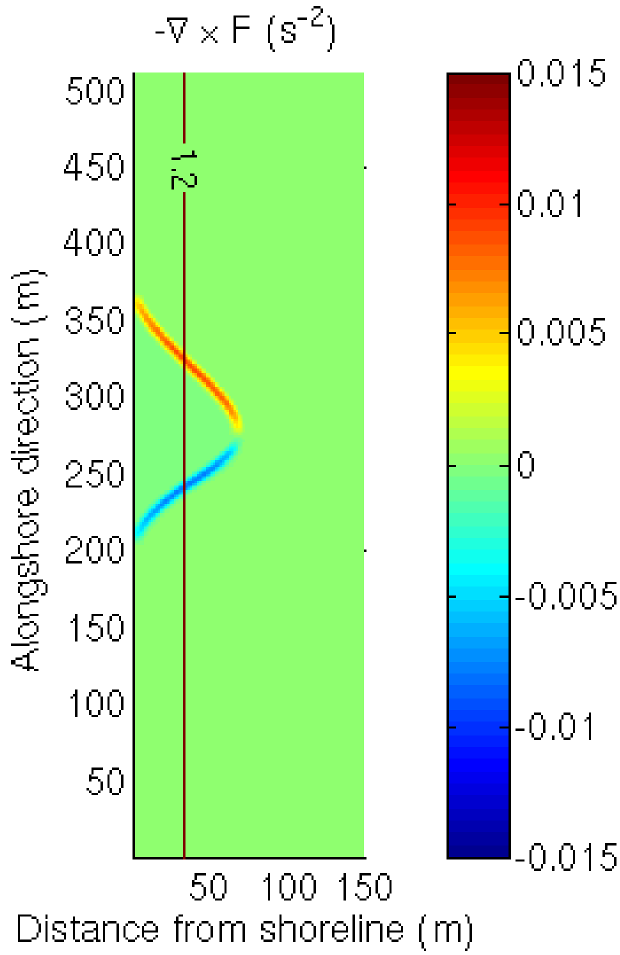

Figure 3. $-\nabla \times F$ for simulation C

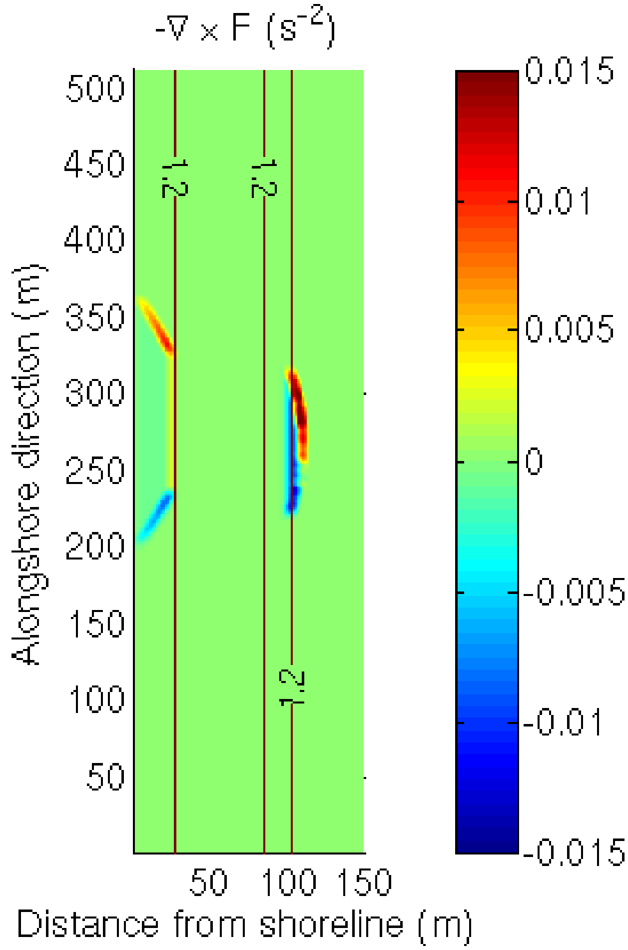

Figure 4. $-\nabla \times F$ for simulation A

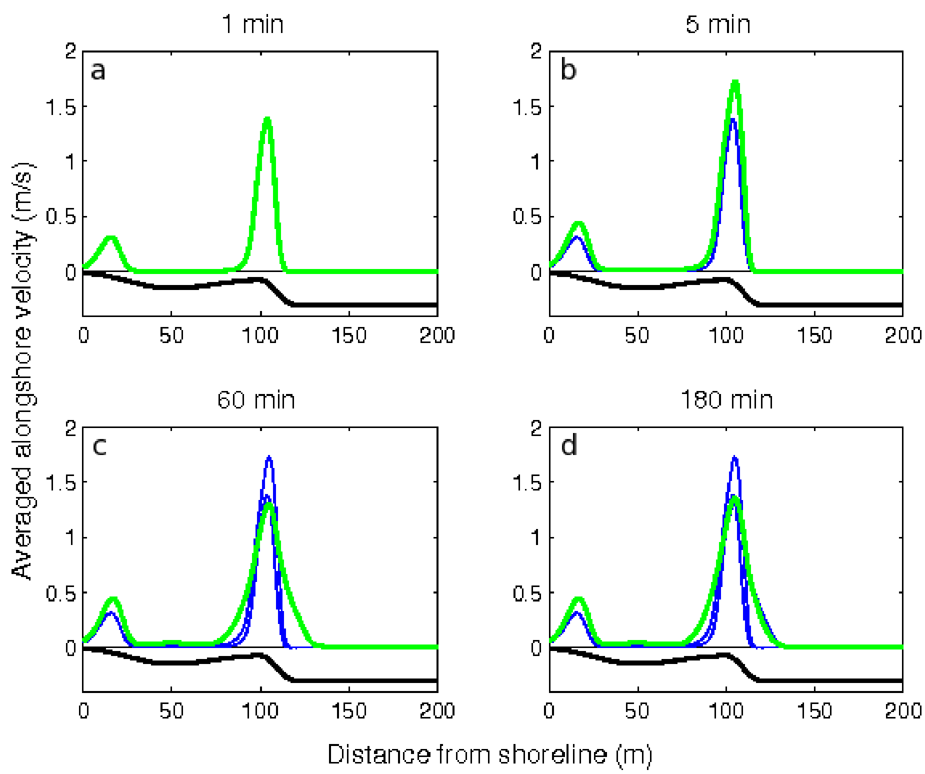

Figure 5. Early development of alongshore-averaged longshore velocity for simulation B. The heavy line denotes the velocity profile at the time indicated in the subplot title. In subplots (b), (c), and (d), thinner lines indicate the earlier velocity profiles for comparison. A scaled plot of the bathymetry is shown below the zero velocity line.

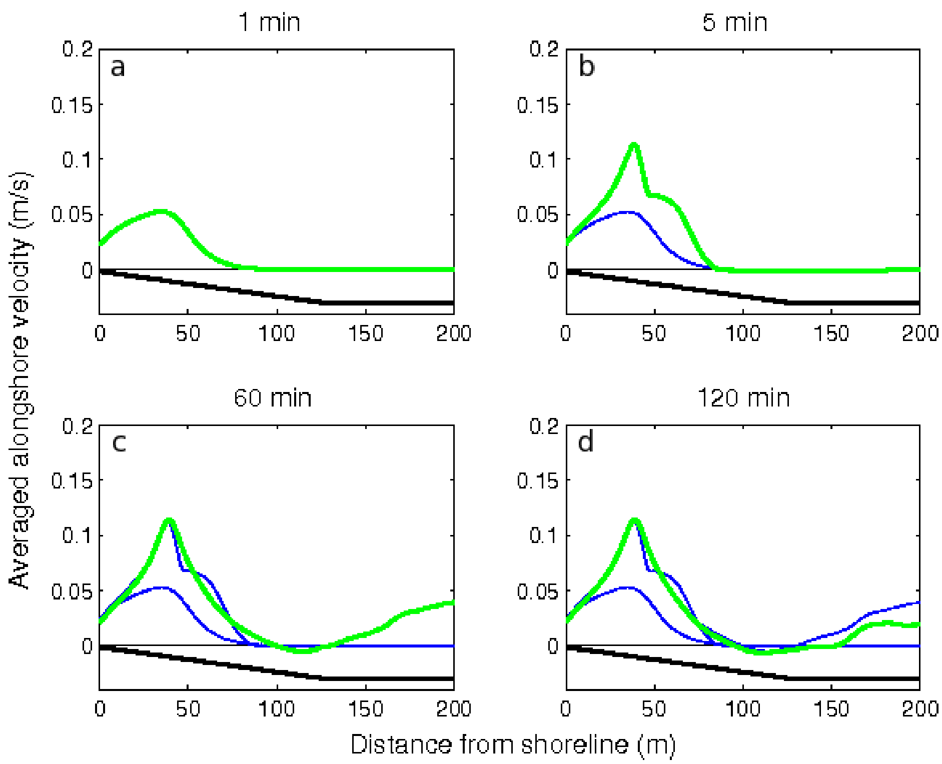

Figure 6. Early development of alongshore-averaged longshore velocity for simulation C. The heavy line denotes the velocity profile at the time indicated in the subplot title. In subplots (b), (c), and (d), thinner lines indicate the earlier velocity profiles for comparison.

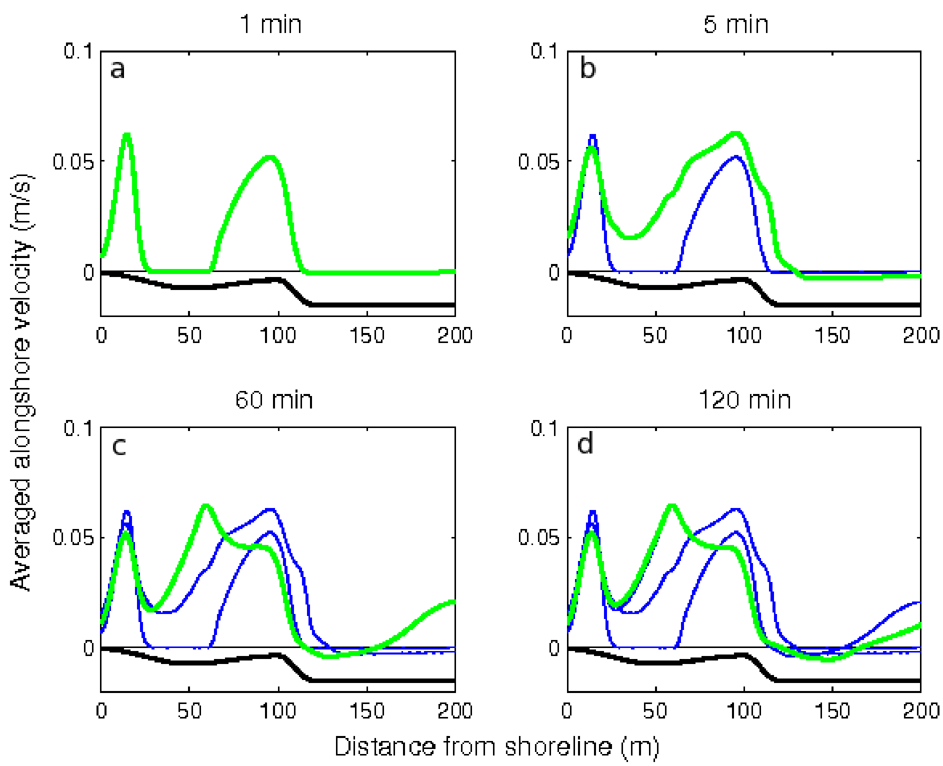

Figure 7. Early development of alongshore-averaged longshore velocity for simulation A. The heavy line denotes the velocity profile at the time indicated in the subplot title. In subplots (b), (c), and (d), thinner lines indicate the earlier velocity profiles for comparison.

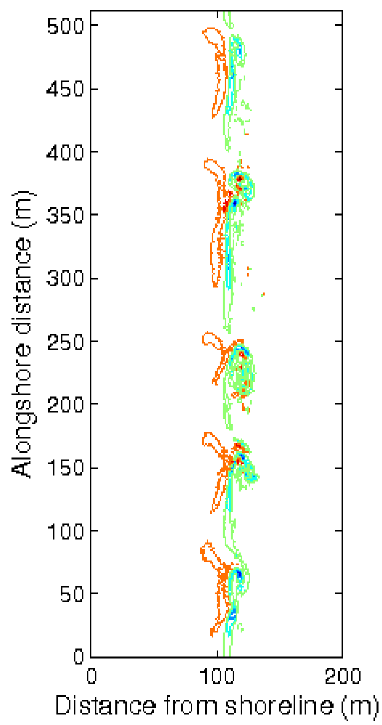

Figure 8. Potential vorticity snapshot from simulation B.

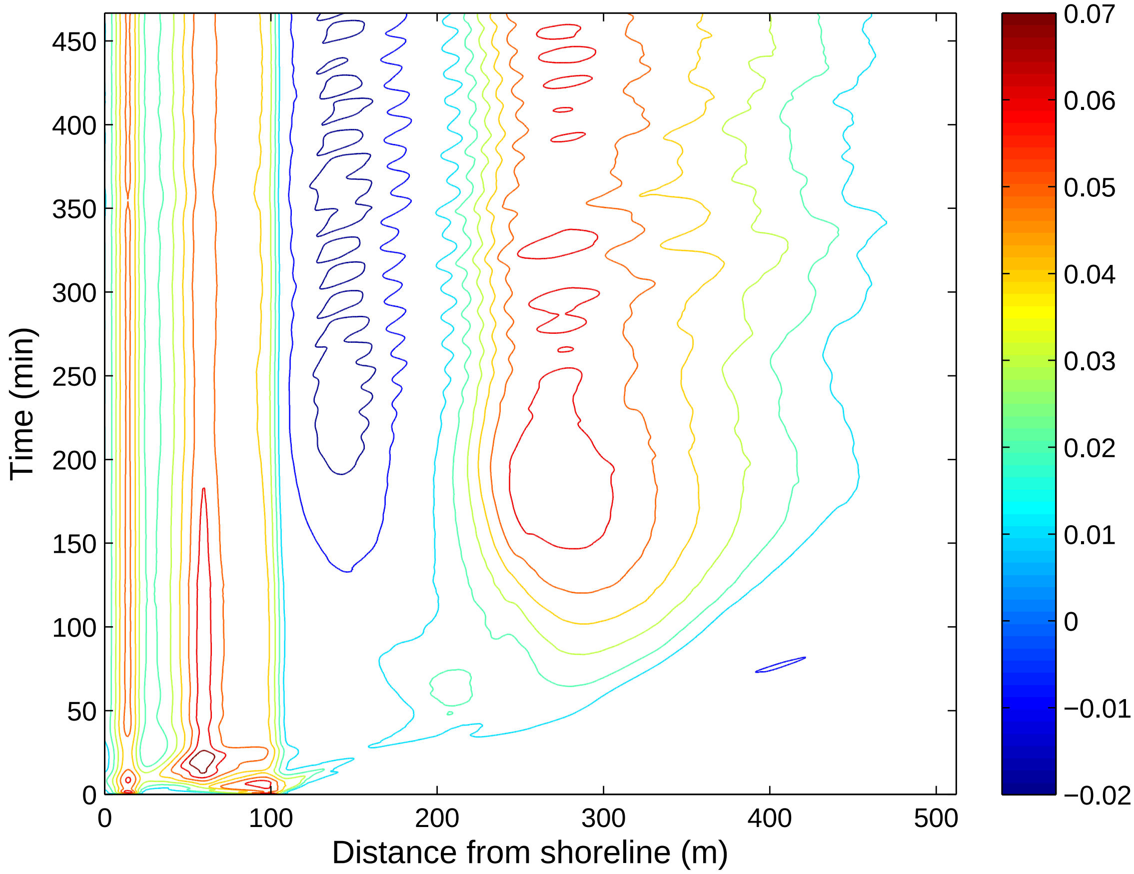

Figure 9. Alongshore-averaged alongshore velocity for simulation A.

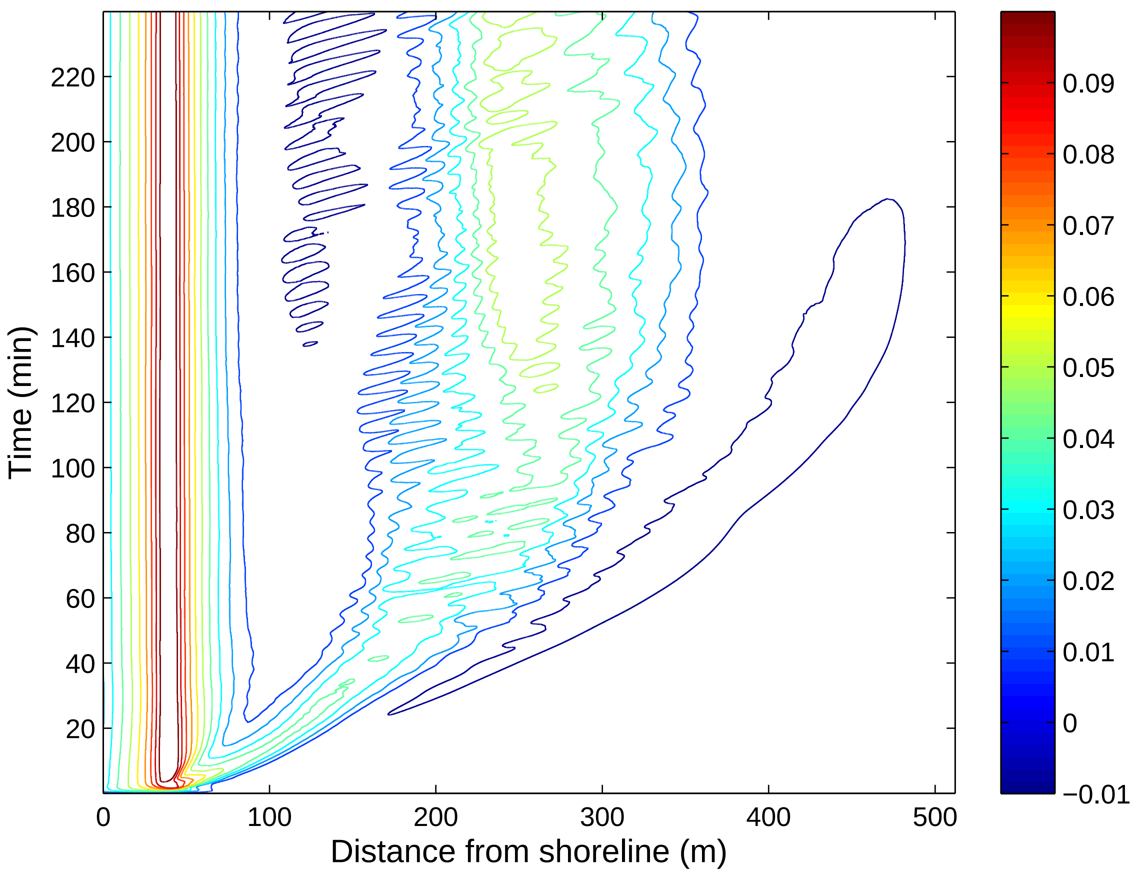

Figure 10. Alongshore-averaged alongshore velocity for simulation C.

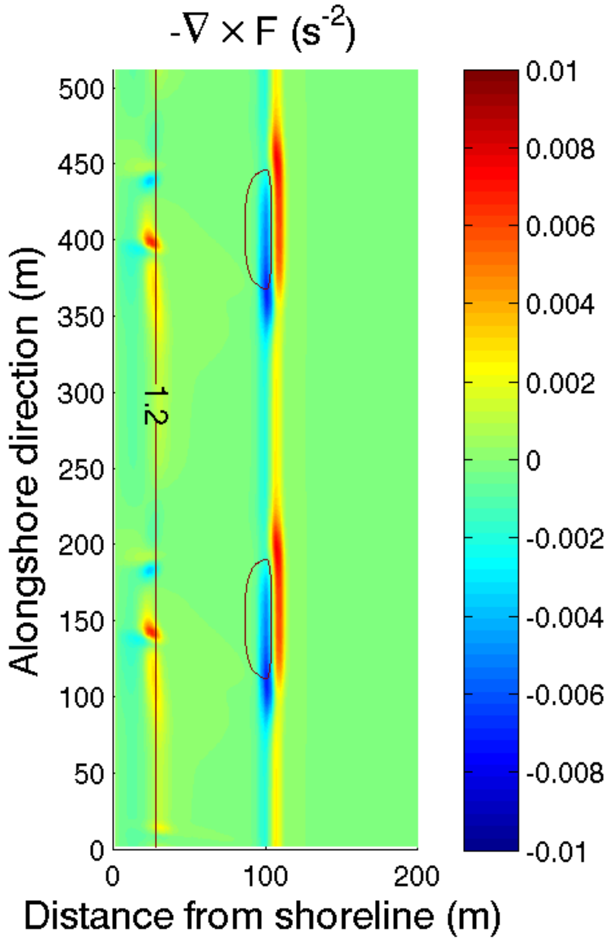

Figure 11. $-\nabla \times F$ for simulation E

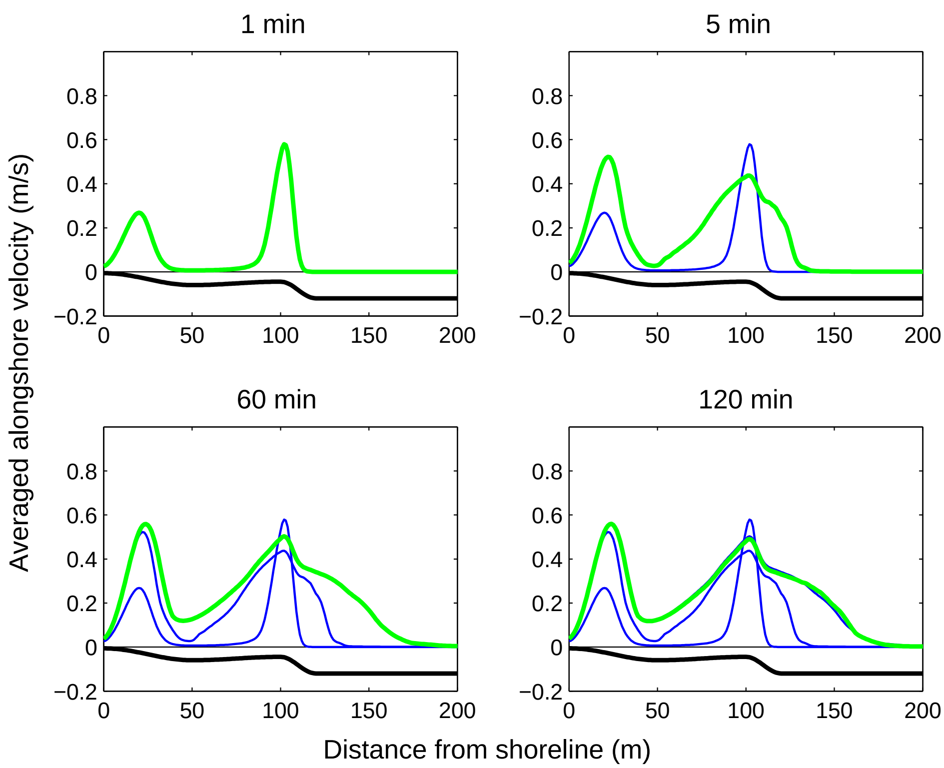

Figure 12. Early development of alongshore-averaged longshore velocity for simulation E. The heavy line denotes the velocity profile at the time indicated in the subplot title. In subplots (b), (c), and (d), thinner lines indicate the earlier velocity profiles for comparison.

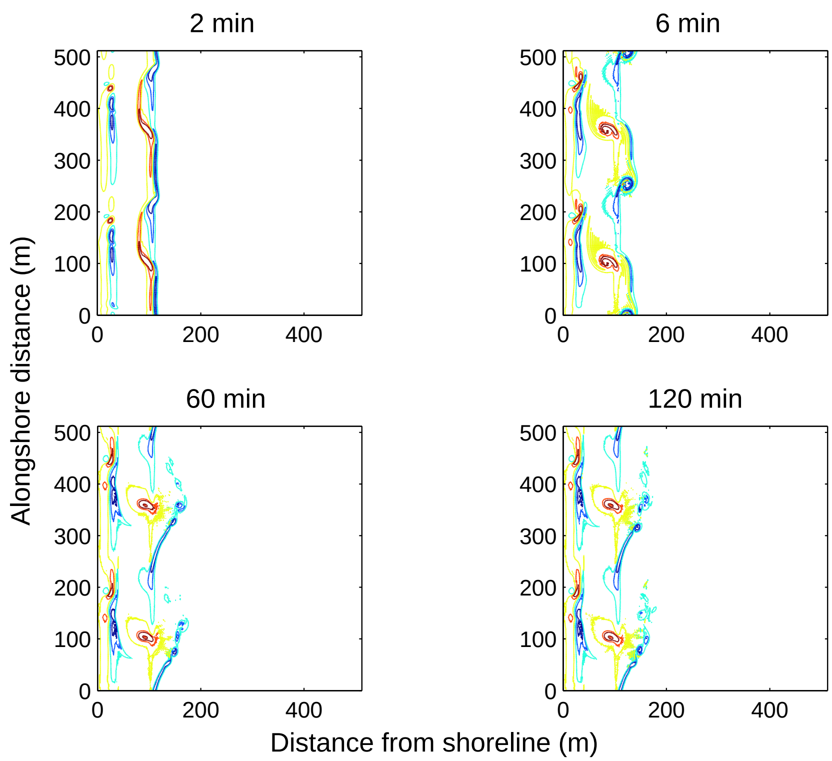

Figure 13. Potential vorticity snapshots from simulation E